Appl. Phys. A 89, 127–132 (2007)
DOI: 10.1007/s00339-007-4152-0

Applied Physics A
Materials Science & Processing

J. BURGHOFF[1,✉]
S. NOLTE[1]
A. TÜNNERMANN[1,2]

Origins of waveguiding in femtosecond laser-structured $LiNbO_3$

[1] Institut für Angewandte Physik, Friedrich-Schiller-Universität Jena, Max-Wien-Platz 1, 07743 Jena, Germany
[2] Fraunhofer-Institut für Angewandte Optik und Feinmechanik, Albert-Einstein-Straße 7, 07745 Jena, Germany

Received: 31 May 2007/Accepted: 4 June 2007
Published online: 28 June 2007 •

ABSTRACT Femtosecond laser-induced structural changes in $LiNbO_3$ are studied. Depending on the laser processing parameters two different types of modification are identified and their origin is discussed. Both types of modification can be described within the framework of induced lattice defects. For strong material damage a refractive index increase can be obtained due to the induced stress field. By appropriate tailoring of this stress field thermally stable and highly symmetric waveguides can be obtained well suited for nonlinear integrated-optical applications.

PACS 61.80.Ba; 77.84.Dy; 42.65.Re; 42.82.Et

1 Introduction

Lithium niobate ($LiNbO_3$) is one of the most important materials for integrated-optical applications due to its wide transparency range and its outstanding electrooptic and nonlinear properties. Although mature technologies exist for waveguide fabrication [1], the inherent capability of the femtosecond laser direct-write method to produce three-dimensional structures [2, 3] has triggered ongoing research in this direction.

Soon after the initial demonstration of optical waveguiding in $LiNbO_3$ induced by focused femtosecond laser pulses [4], two distinct types of modification were observed that showed fundamentally different structural properties [5, 6]. It was shown that the temporal width of the ultrashort pulses had a strong influence on the resulting structures [7]. Detailed investigations on the structural and optical properties of the two types of modification were given [8]. Here, we will focus on the origin of the different types of modification with respect to their waveguiding properties. We will show that both modifications can be understood by a common model of lattice defects. Pathways for obtaining highly stable and symmetric waveguides without any loss of nonlinearity will be given.

2 Experimental

For the structuring of the $LiNbO_3$ crystals a commercial amplified Ti:sapphire femtosecond laser system (Spectra-Physics, Spitfire) was used. The system was operated at a repetition rate of 1 kHz and provided pulses at a central wavelength of 800 nm with a minimum pulse duration of 35 fs and pulse energies up to 1 mJ. For obtaining longer pulse durations the grating compressor was misadjusted. A continuous variation of the output power was obtained by using a motorized half-wave plate and a subsequent polarizer. The laser was focused into the sample with a 40× microscope objective (NA = 0.65) within a depth of 50–150 μm below the sample surface. In order to produce straight lines of modification as required for waveguiding the sample was moved perpendicular to the laser beam axis with a velocity of 100 μm/s using an air-bearing xyz positioning system (Aerotech, ABL90030).

The $LiNbO_3$ samples were congruent x- and z-cut samples from Crystal Technology. After laser processing the end facets were polished and inspected by optical microscopy. To evaluate the induced refractive index changes thin slices of the sample were cut and polished down to a thickness of 40 μm. These slices were analyzed using a shearing interferometric microscope at 550 nm. For the characterization of the waveguiding properties laser light at 633 nm and 1.06 μm was fiber-coupled into the structures and the end facet was imaged onto a CCD camera.

3 Results and discussion

The illumination of $LiNbO_3$ with ultrashort laser pulses results in structural modifications which can be used to fabricate optical waveguides. Depending on the processing parameters like pulse energy, pulse duration or numerical aperture of the focusing lens, two types of structure can be distinguished. Figure 1 shows examples of the refractive index distribution and guided optical mode field for each type in an x-cut sample. To choose which kind of structure was obtained, only the pulse duration was varied. As was explained in detail in [8], the nonlinear propagation of the pulse strongly influences the spatial distribution of the energy density in the focus. This is a result of the effects of self-focusing and defocusing due to the created plasma. At pulse durations of the order of 100 fs and the experimental conditions described here,

✉ Fax: +49 3641 947802, E-mail: burghoff@iap.uni-jena.de

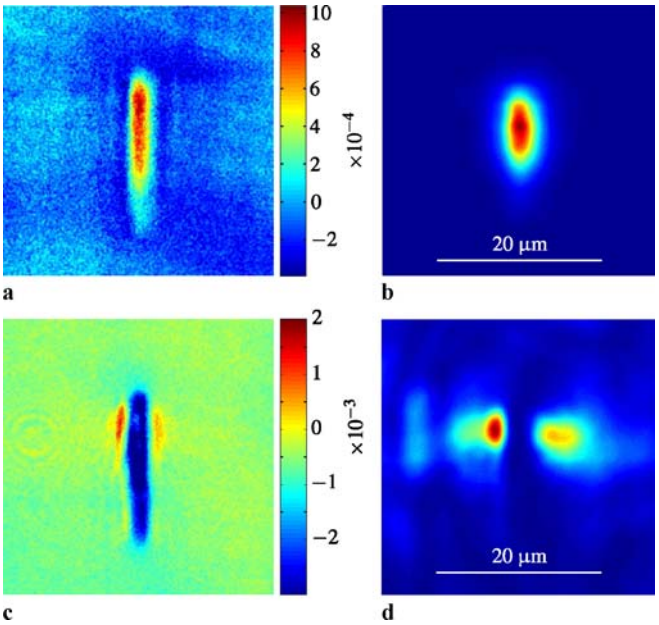

FIGURE 1 Two types of waveguides in x-cut $LiNbO_3$ at a fixed pulse energy of 0.2 µJ and different pulse widths. (**a**) Extraordinary refractive index profile and (**b**) guided optical mode at a wavelength of 633 nm for a pulse duration of 220 fs (type I); (**c**) extraordinary refractive index profile and (**d**) guided optical mode for a pulse duration of 1.1 ps (type II)

the intensity reaches the threshold for nonlinear absorption well before the focus so that the energy is deposited in a large volume. As a consequence, the deposited energy in the focal volume is low resulting in only weak damage. This weak damage coincides with an increase of the extraordinary refractive index n_e as can be seen in Fig. 1a. No noticeable change of the ordinary refractive index n_o is observed in this case. We will refer to this type of modification as type I in the following.

In contrast, for pulses of equal energy but picosecond duration, nonlinear absorption does not set in until the focus is reached. Thus a much higher fluence is obtained in this case resulting in strong material damage and a decrease of both ordinary and extraordinary refractive index. As can be seen in Fig. 1c, this is accompanied by a refractive index increase at the sides of the damaged region which gives rise to waveguiding (type II). Similar observations have been made in other crystalline materials [9–11], suggesting a common mechanism underlying this behavior.

The two types of structural modification have been shown to exhibit quite different physical properties. Only a short summary of them is given here while the origin of the waveguiding is discussed in detail. In Sect. 3.1, the mechanisms responsible for the extraordinary index increase at low fluences are proposed. The relation of the decrease of the refractive index at high fluences to stress in the crystalline lattice along with numerical simulations of the resulting waveguides are presented in Sect. 3.2.

3.1 *Origin of the extraordinary index increase*

The first type of modification, shown in Fig. 1a, is characterized by an increase of the extraordinary refractive index in the focal volume while the ordinary index is unchanged. It occurs only in regions of moderate laser fluence. At elevated temperatures of 200 °C, the structures completely vanish. Moreover, the electrooptic properties of such waveguides are markedly reduced [8].

A number of mechanisms may cause an increase of n_e. Among those are the photorefractive effect, changes in chemical composition and lattice defects. The following discussion will show that only lattice defects can explain the full set of observations.

The photorefractive effect appears as a change of refractive index when the sample is illuminated with light in the visible spectral range. Absorption at Fe^{3+} impurities creates conduction band electrons that move along the crystal c direction by means of the bulk photovoltaic effect [12]. This results in space charges that alter the refractive index via the electrooptic effect. Under inhomogeneous illumination, the electrons move out of the irradiated volume and get trapped nearby causing a refractive index profile that shows a characteristic decrease in the center along with smaller positive wings [13]. Moreover, the shape of the refractive index profile is the same for both n_o and n_e while the amplitude is different. Under near-infrared femtosecond illumination, where the absorption process is nonlinear, time constants for this process of the order of minutes have been observed [14]. This is in contrast with the results reported here, where one point of a waveguide is irradiated with only a few pulses and therefore exposure times of some milliseconds are obtained. Furthermore, the characteristics of the photorefractive effect are not in agreement with the refractive index changes shown in Fig. 1 as isolated regions of increased n_e are observed. Moreover, experiments performed in MgO-doped $LiNbO_3$, where the photorefractive effect is orders of magnitude smaller, revealed similar modifications after femtosecond laser irradiation. Thus the influence of the photorefractive effect is considered negligible.

The increase of n_e may also be caused by ion migration resulting in changes of the chemical composition. In $LiNbO_3$, the most mobile ion species are Li as well as H which is always present in the crystal as an impurity. For $\Delta n_e > 0$ an increased concentration of H ions is necessary [15]. However, the high temperatures during the laser structuring suggest diffusion out of the modified volume. Thus, the influence of H ions can be ruled out. In contrast, diffusion of Li ions out of the irradiated volume can explain an increase of n_e [16]. For ultraviolet laser structuring of $LiNbO_3$, it was proposed that the Li ions diffuse due to a temperature gradient induced by the local laser absorption [17]. In the case of femtosecond laser structuring at kilohertz repetition rates, this mechanism yields no satisfactory explanation as the following calculation according to [18] shows. Under the ideal assumption that

the absorbed energy of the pulse heats the crystal instantaneously at one point, the heat conduction can be modeled by the heat conduction equation [19]. The calculation shows that after a time of 10 µs, the temperature has already fallen below 300 K for an absorbed energy of 1 µJ. The ions are thus mobile only during this period of time in which the temperature gradient exists. The ion diffusion is calculated by the diffusion equation which is analogous to the heat conduction equation. In a time τ, the ions can travel a characteristic distance $l_D \approx 2(D\tau)^{1/2}$. At a temperature of 1000 K the diffusion constant D has a value of $D = 2 \times 10^{-14}\,m^2/s$ for Li ions [18]. Consequently, during the time $t = 10\,\mu s$ calculated above these ions can travel only as far as $l_D \approx 1$ nm. This value illustrates that the time of elevated temperature is insufficient for ion diffusion to take place. In the experiments, each spot was irradiated with approximately 10 pulses, so that accumulation effects should not be important.

Defects in the crystalline lattice can have a significant influence on the optical properties of $LiNbO_3$. This was extensively investigated in connection with the implantation of ions. There, several features were observed that are shortly summarized in the following.

When high energy ions impinge on the crystal they are slowed down by lattice interactions until they are halted in a depth t_n. This depth is characteristic of the ion species and its energy [20]. While for the fast ions the energy loss is dominated by electronic interactions, elastic collisions with the lattice atoms become dominant when the ions have lost most of their energy. Correspondingly, two regions with different properties are created giving rise to different optical properties. The resulting extraordinary index profiles are schematically shown in Fig. 2 as a function of depth. For high doses (solid line), both indices of refraction exhibit a strong decrease in a depth t_n, i.e. at the end of the ion track (region II). In contrast, an increase only of the extraordinary index can be observed in the region of electronic interaction (region I) in $LiNbO_3$ [21].

Structural investigations showed strong damage of the crystalline structure in region II. This explains the index decrease which is due to a reduction in density as a result of the defects. In addition, it can be observed that the nonlinear properties are completely removed. Full recovery is impossible even when annealing at 500 °C [22].

A different behavior is observed in region I. Here, the lattice structure is still intact with the exception of point defects. Although the nonlinearity is reduced in this case as well, it could be completely restored by annealing at temperatures of 200 °C [22]. Unfortunately, no detailed information is available about the temperature stability of the refractive index changes in this region.

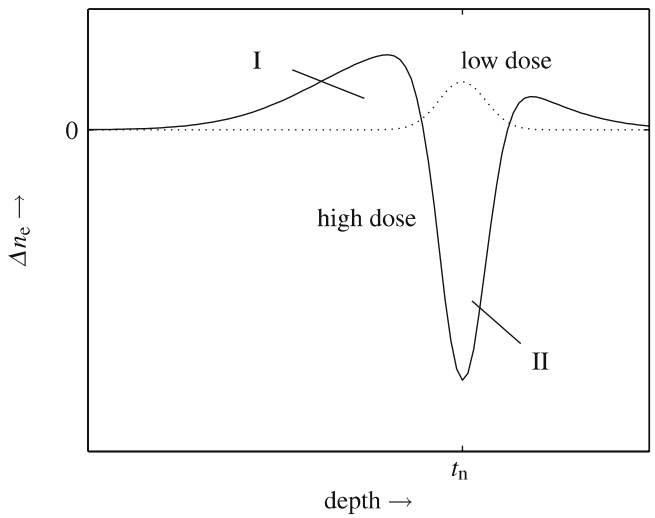

FIGURE 2 Schematic of the extraordinary index profile after the implantation of ions (*solid line*: high dose; *dotted line*: low dose) into $LiNbO_3$ (after Rams et al. [21]). The nuclear damage region is located at a depth t_n

Similar results as observed in region I can be obtained at the end of the ion track (region II) when only low doses are used. The extraordinary index is enhanced in this case in region II, while the ordinary index still shows a decrease. No refractive index changes can be observed in region I [21]. This is consistent with the weak lattice damage observed in region I when exposing the sample with high doses.

To explain the increase of n_e several mechanisms were proposed. Firstly, a defect-induced increase of ion mobility could cause Li ions to move into the nuclear damage zone (region II). Accordingly, this would leave regions of depleted Li concentration resulting in an enhancement of n_e [16]. However, this does not explain the increase of the extraordinary index in the damage region at low doses. Secondly, it was assumed that lattice defects lower the spontaneous polarization of the crystal. The spontaneous polarization P_s is the result of the permanent electric dipole moment in the ferroelectric phase which is caused by the dislocation of Li and Nb atoms with respect to the oxygen octaeders [23]. The refractive index is reduced because of P_s due to the quadratic electrooptic effect [24, 25]:

$$\delta n_o = -\frac{1}{2} n_o^3 g_{13} P_s^2 ,$$
$$\delta n_e = -\frac{1}{2} n_e^3 g_{33} P_s^2 , \qquad (1)$$

where g is the quadratic electrooptic coefficient. With values of $\delta n_o = -0.06$ and $\delta n_e = -0.24$ this gives rise to the large negative birefringence observed in $LiNbO_3$. Consequently, a reduction of P_s would therefore mainly result in an increase of n_e. This is counteracted by the enlargement of the unit cell and thus an increase of the molar volume due to a reduction of crystallinity. In a simplified model, this can be related to a decrease of refractive index by the Clausius–Mosotti equation [26]:

$$\frac{n^2 - 1}{n^2 + 2} = \frac{\alpha_M}{V_M} . \qquad (2)$$

Here, α_M denotes the molar polarizability. The combination of volume change and decrease of spontaneous polarization was deemed responsible for the observed index changes caused by ion implantation [27, 28]. Note that a similar

discussion has also been made for proton exchange [29].

While quantitative predictions are impossible due to the simple nature of the model, qualitatively, the increase of n_e at low damage, i.e. in region I or at low doses, is plausible. In this case the lattice structure is still preserved and thus the volume increase is negligible. When the damage is stronger, the volume change becomes the dominant contribution so that both indices of refraction are decreased.

The phenomena observed with ion implantation and the proposed induced damage model offer a striking analogy to femtosecond laser structuring. The question if type I or II structures are induced by the laser can thus be answered based on the degree of the resulting damage. For pulse durations of ≈ 100 fs or within filaments, the laser fluence is kept at a moderate level thereby creating limited damage [8]. In this case, type I modifications with $\Delta n_e > 0$ occur. If the pulse duration is of the order of 1 ps or in filaments with repeated self-focusing at powers much higher than the critical power, the fluence exceeds the threshold for catastrophic collapse so that strong damage of the crystal is induced. Therefore, type II structures with a decrease of both indices occur in this case.

This model is also in agreement with the observed temperature behavior of the modifications. The thermal erasure of type I waveguides coincides with the annealing of isolated point defects at temperatures of 200 °C [22]. In addition, the loss of nonlinearity can be explained by the decrease of spontaneous polarization since the electrooptic and nonlinear properties depend linearly on P_s in this class of crystals [30].

3.2 *Waveguiding based on stress-induced refractive index changes*

When $LiNbO_3$ is subjected to high laser energy densities, as obtained in the focus for example by using picosecond pulses, both indices of refraction are decreased (type II modification, see Fig. 1c). However, regions with increased refractive index are obtained adjacent to the modifications allowing to guide light (Fig. 1d). These structures were shown to be stable up to temperatures of > 300 °C [8].

Within the model of lattice defects, this type of modification can be readily explained: the high laser fluences lead to strong disorder of the crystal resulting in a volume increase. As a result the refractive index is decreased according to (2). At the same time, stress is induced in the surrounding material. Here, it is assumed that the elastooptic effect is responsible for the observed refractive index changes in analogy to previous publications on quartz [9, 31]. In this section we present numerical simulations of the stress-induced refractive index changes and the resulting guided-optical mode fields and discuss the implications for practical waveguide fabrication.

The simulation relies on the shape of the modified region which is determined by the numerical aperture of the focusing objective and nonlinear processes. For simplicity, an ideal elliptical shape was assumed with typical diameters of $a = 15\,\mu$m along the direction of laser incidence and $b = 2.5\,\mu$m perpendicular to it. To estimate the volume change of the structured region, the differential form of (2) is used:

$$\frac{\Delta V}{V} = -\frac{6n}{(n^2+2)(n^2-1)}\Delta n \approx -0.5\Delta n\,. \tag{3}$$

For experimentally observed ordinary refractive index changes of the order of -10^{-2} this yields relative volume changes of some 10^{-3}. Note that this is only a qualitative estimation, since other mechanisms of refractive index change have been neglected. Furthermore, it was assumed that the structures are homogeneous along the waveguide direction. In the absence of cracks, this is ensured by the overlap of multiple pulses at one position. Under these conditions the problem can be simplified to a planar geometry. Finite element calculations were carried out with the software Comsol Multiphysics [32] using a plain strain model. Within this model, the strain tensor is planar while a nonzero component of the stress tensor along the waveguide direction (σ_{zz}) exists. The volume change of the elliptical modification was simulated by thermal expansion to an arbitrary temperature at which $\Delta V/V = \Delta a/a + \Delta b/b$ had reached the desired value.

The stress distribution in the crystal surrounding the structured region was calculated with a relative volume change of $\Delta V/V = 7 \times 10^{-3}$. We do not provide a graph of the stress here since it resembles the refractive index profiles of Fig. 3a and b. At the sides of the modification compressive stress exists in the horizontal direction as well as tensile stress in the vertical direction; its magnitude is of the order of 10 MPa.

Refractive index changes were calculated from the stress values σ_{kl} using

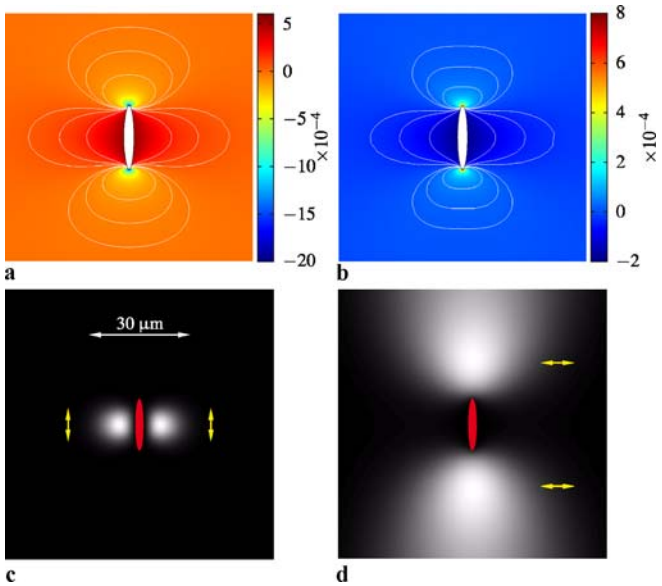

FIGURE 3 Calculated refractive index profiles (**a**) Δn_x for vertical (TM) and (**b**) Δn_z for horizontal polarization (TE) according to the induced stress. This results in the optical mode fields for a wavelength of 633 nm for (**c**) TM and (**d**) TE polarization, respectively

the piezooptic effect [33]:

$$\Delta\left(\frac{1}{n^2}\right)_{ij} = \sum_{k,l} \pi_{ijkl}\sigma_{kl} = \sum_{m,n,k,l} p_{ijmn}s_{mnkl}\sigma_{kl} \,. \quad (4)$$

Here, the piezooptic tensor $\pi_{ijkl} = \sum_{m,n} p_{ijmn}s_{mnkl}$ is evaluated from literature values of the elastooptic tensor p and the elastic compliance tensor s [23]. The result is shown in Fig. 3a and b. At the sides of the structure, the index change is positive for vertical (TM) and negative for horizontal polarization (TE); above and below the ellipse the signs are opposite. Based on the refractive index profiles, the optical mode fields were calculated for a wavelength of 633 nm. Each polarization was treated separately. It was further assumed that within the structure, the index change was -10^{-2} for TM and half this value for TE polarization, in accordance with [8]. In the simulation, off-diagonal elements of the tensor $(1/n^2)_{ij}$ were neglected for technical reasons. The results are shown in Fig. 3c and d. Well-confined guiding exists at the side of the ellipse for TM-polarization. For TE-polarization, where the regions of increased index are located above and below the structure, the guiding is weak and the corresponding mode field very large. The reason for this is that the index increase at the tip of the ellipse is limited to a small area, although its magnitude is greater than for TM-polarization. Note, however, that this is strongly dependent on the assumed shape of the ellipse.

The results of Fig. 3 are based on the geometry of an x-cut crystal with the waveguide direction along y. For other geometries, similar results were obtained with strong TM guiding at the side of the ellipse and weak TE guiding above and below. The accentuation of the lateral regions for strong guiding is owed to the shape and orientation of the ellipse, however. If in the simulation the ellipse is rotated by 90°, then the regions of strong guiding are located above and below while the polarizations are maintained. This illustrates that with adequate beam shaping, the waveguiding properties can be specifically tailored. For more complex shapes of the modifications, as are observed in filaments, multiple regions of TE and TM guiding in close proximity may be observed so that no simple predictions can be made.

The available experimental data is in agreement with the results of the simulation. Nejadmalayeri et al. reported TM guiding at the sides and TE guiding below laser-induced modifications in z-cut $LiNbO_3$ [7]. These waveguides exhibited propagation losses as low as 0.7 dB/cm. Moreover, the observations in crystalline quartz [9, 31] can also be interpreted by the model for $LiNbO_3$ as both crystals show the same symmetry in their elastic and elastooptic tensors.

The waveguides that are based on stress in the crystal are inherently unsymmetric since they are always located next to the modification whose decreased refractive index acts as a strong barrier for the guided mode. For integrated-optical elements, however, symmetric modes are mandatory to ensure a high coupling efficiency to optical fibers. To fabricate symmetric waveguides with high thermal stability, we demonstrated the approach of writing two parallel lines in close separation [34, 35]. In this case the TM guiding regions overlap and form a well-confined waveguide in the center between the lines. In Fig. 4, simulation results for this geometry and a separation of 10 µm are shown. In the calculation, the single modifications were modeled in the same way as in Fig. 3. For TM polarization, a homogeneous index increase in the center is created. As can be seen in Fig. 4b, this region is limited both in horizontal and vertical direction by barriers of decreased index. The calculated mode field in Fig. 4c thus shows a high confinement and symmetric shape. For small separations ≤ 6 µm, no central mode is guided. In the other extreme, two separate modes exist for large separations. Depending on the wavelength, the magnitude of the index changes and the line separation, the guiding of higher order modes is also possible.

To verify the above considerations, waveguides were produced in x-cut $LiNbO_3$ using a pulse energy of 0.3 µJ and a pulse duration of 1.2 ps. These parameters resulted in strong material damage with a smooth elliptical shape. As can be seen in Fig. 5a, a single line exhibited the typical guiding properties for TM polarization similar to Fig. 3c. When two lines were fabricated with a separation of 10 µm, a symmetric mode with better confinement emerged in the center (Fig. 5b). If the polarization was adjusted to TE, no guiding could be observed.

The damping losses of these waveguides were then measured by comparing the transmitted light to the light reflected back out of the waveguide when

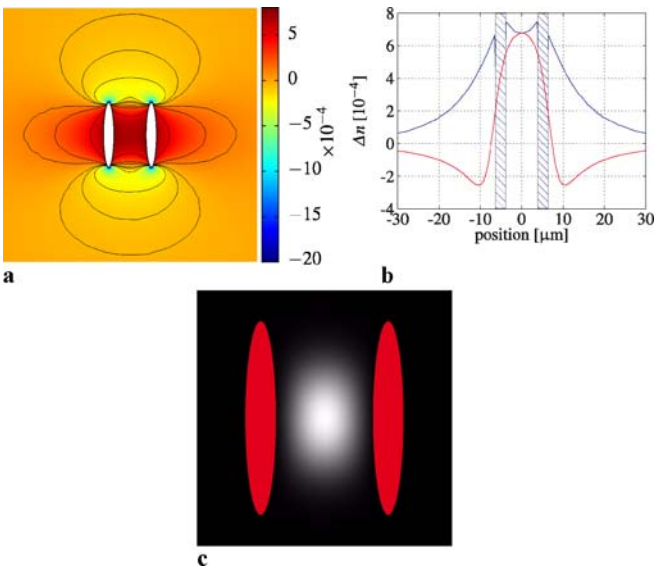

FIGURE 4 (**a**) Simulated refractive index distribution for TM polarization for a double line structure with 10 µm separation. The single modifications were modeled in the same way as in Fig. 3. (**b**) Horizontal (*blue*) and vertical (*red*) cross section of the refractive index profile. Note that there is a strong refractive index decrease (10^{-2}) in the destructed elliptical zones (*shaded regions*). (**c**) Resulting mode profile for TM polarization at a wavelength of 633 nm

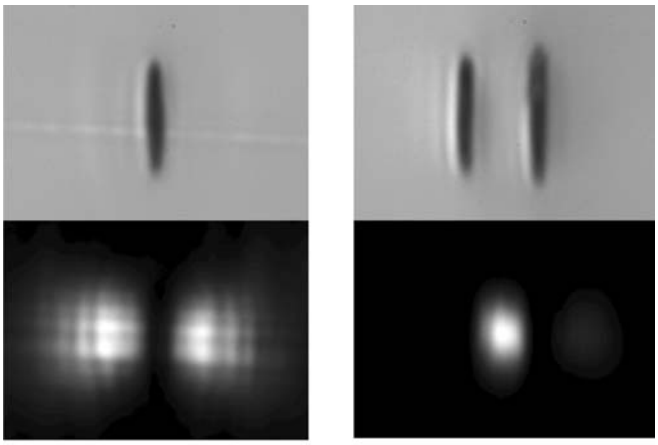

a b

FIGURE 5 Experimental comparison of the optical guiding properties of (**a**) a single line and (**b**) a double line structure with 10 μm separation in x-cut $LiNbO_3$. The modifications have been induced with a pulse energy of 0.3 μJ, a pulse duration of 1.2 ps and a scan speed of 1 mm/s. In this case a Ti:sapphire laser system operating at 100 kHz has been used. At the top microscope images of the induced structures are shown. The dimensions of each modification are $2 \times 13\ \mu m^2$. At the bottom the near-field intensity distributions are given for a wavelength of 633 nm and TM polarization. Light propagation is along the z-axis

a high-reflectivity mirror was positioned at the sample end facet. At the wavelength of 1.06 μm used, a line separation of 17 μm showed the best guiding. With this setup the propagation losses were measured to be ≈ 0.6 dB/cm.

4 Conclusions

The mechanisms which lead to refractive index changes have been discussed for the two observed types of fs laser-induced structures in $LiNbO_3$ for the first time to the authors' knowledge. Both types are well explained by the model of lattice defects at different degrees of damage. For lower laser fluences, point defects are created which lower the spontaneous polarization of the crystal and thus increase the extraordinary index. Strong crystalline damage at high fluences leads to a volume increase that correlates with diminished refractive indices. It has been shown that the latter mechanism also explains stress-induced refractive index changes in the vicinity of the structure. Using finite element simulations, the shape and polarization dependence of the guided modes could be modeled in agreement with experimental observations. Due to the general nature of the process, these results are also valid for other crystalline materials.

It has been demonstrated by experiment and simulation that by fabricating two parallel lines close to each other, low-loss symmetric waveguides are created. Unlike waveguides based on an increased extraordinary refractive index, the former are thermally stable and do not suffer from a diminished nonlinearity. The results given here thus permit to further improve the performance of femtosecond laser-written waveguides in $LiNbO_3$ in order to fabricate efficient nonlinear integrated-optical devices.

ACKNOWLEDGEMENTS Financial support by Schott AG and the Deutsche Forschungsgemeinschaft under priority program 1157 is gratefully acknowledged.

REFERENCES

1 Y.N. Korkishko, V.A. Fedorov, *Ion Exchange in Single Crystals for Integrated Optics and Optoelectronics*, 1st edn. (Cambridge International Science Publishing, 1999)
2 K.M. Davis, K. Miura, N. Sugimoto, K. Hirao, Opt. Lett. **21**, 1729 (1996)
3 S. Nolte, M. Will, J. Burghoff, A. Tünnermann, Appl. Phys. A **77**, 109 (2003)
4 L. Gui, B. Xu, T.C. Chong, IEEE Photon. Technol. Lett. **16**, 1337 (2004)
5 R.R. Thomson, S. Campbell, I.J. Blewett, A.K. Kar, D.T. Reid, Appl. Phys. Lett. **88**, 111 109 (2006)
6 J. Burghoff, C. Grebing, S. Nolte, A. Tünnermann, Appl. Surf. Sci. (2007) DOI: 10.1016/j.apsusc.2007.02.148
7 A.H. Nejadmalayeri, P.R. Herman, Opt. Lett. **31**, 2987 (2006)
8 J. Burghoff, H. Hartung, S. Nolte, A. Tünnermann, Appl. Phys. A **86**, 165 (2007)
9 T. Gorelik, M. Will, S. Nolte, A. Tünnermann, U. Glatzel, Appl. Phys. A **76**, 309 (2003)
10 V. Apostolopoulos, L. Laversenne, T. Colomb, C. Depeursinge, R.P. Salathé, M. Pollnau, R. Osellame, G. Cerullo, P. Laporta, Appl. Phys. Lett. **85**, 1122 (2004)
11 A.H. Nejadmalayeri, P.R. Herman, J. Burghoff, M. Will, S. Nolte, A. Tünnermann, Opt. Lett. **30**, 964 (2005)
12 K. Buse, Appl. Phys. B **64**, 273 (1997)
13 F.S. Chen, J. Appl. Phys. **40**, 3389 (1969)
14 O. Beyer, I. Breunig, F. Kalkum, K. Buse, Appl. Phys. Lett. **88**, 051 120 (2006)
15 Y.N. Korkishko, V.A. Fedorov, J. Appl. Phys. **82**, 1010 (1997)
16 U. Schlarb, K. Betzler, Phys. Rev. B **48**, 15 613 (1993)
17 S. Mailis, C. Riziotis, I.T. Wellington, P.G.R. Smith, C.B.E. Gawith, R.W. Eason, Opt. Lett. **28**, 1433 (2003)
18 A. Muir, G. Daniell, C. Please, I. Wellington, S. Mailis, R. Eason, Appl. Phys. A **83**, 389 (2006)
19 D. Bäuerle, *Laser Processing and Chemistry* (Springer, Berlin, 1996)
20 P.D. Townsend, P.J. Chandler, L. Zhang, *Optical Effects of Ion Implantation* (Cambridge University Press, 1994)
21 J. Rams, J. Olivares, P.J. Chandler, P.D. Townsend, J. Appl. Phys. **87**, 3199 (2000)
22 J. Rams, J. Olivares, P.J. Chandler, P.D. Townsend, J. Appl. Phys. **84**, 5180 (1998)
23 R.S. Weis, T.K. Gaylord, Appl. Phys. A **37**, 191 (1985)
24 S.H. Wemple, M. DiDomenico Jr., I. Camlibel, Appl. Phys. Lett. **12**, 209 (1968)
25 K. Sugii, M. Fukuma, H. Iwasaki, J. Mater. Sci. **13**, 523 (1978)
26 C. Gerthsen, *Physik*, 8th edn. (Springer, Berlin, 1964)
27 V.V. Atuchin, Nucl. Instrum. Methods Phys. Res. B **168**, 498 (2000)
28 H. Hu, F. Lu, F. Chen, B.-R. Shi, K.-M. Wang, D.-Y. Shen, Appl. Opt. **40**, 3759 (2001)
29 H. Åhlfeldt, J. Webjörn, P.A. Thomas, S.J. Teat, J. Appl. Phys. **77**, 4467 (1995)
30 M. DiDomenico Jr., S.H. Wemple, J. Appl. Phys. **40**, 720 (1969)
31 M. Will, J. Burghoff, S. Nolte, A. Tünnermann, F. Wunderlich, K. Goetz, Proc. SPIE **5714**, 261 (2005)
32 COMSOL 3.2, http://www.comsol.com
33 J.F. Nye, *Physical Properties of Crystals* (Oxford University Press, Oxford, 1985)
34 S. Nolte, J. Burghoff, M. Will, A. Tünnermann, Proc. SPIE **5340**, 164 (2004)
35 J. Burghoff, C. Grebing, S. Nolte, A. Tünnermann, Appl. Phys. Lett. **89**, 081 108 (2006)